RESEARCH ARTICLE

NODDI in gray matter is a sensitive marker of aging and early AD changes

Xi Yu[1] | Scott A. Przybelski[2] | Robert I. Reid[2,3] | Timothy G. Lesnick[2] | Sheelakumari Raghavan[3] | Jonathan Graff-Radford[4] | Val J. Lowe[3] | Kejal Kantarci[3] | David S. Knopman[4] | Ronald C. Petersen[4] | Clifford R. Jack Jr.[3] | Prashanthi Vemuri[3]

[1]Department of Physiology and Biomedical Engineering, Mayo Clinic, Rochester, Minnesota, USA

[2]Department of Health Sciences Research, Division of Biomedical Statistics and Informatics, Mayo Clinic-Rochester, Rochester, Minnesota, USA

[3]Department of Radiology, Mayo Clinic-Rochester, Rochester, Minnesota, USA

[4]Department of Neurology, Mayo Clinic-Rochester, Rochester, Minnesota, USA

Correspondence
Prashanthi Vemuri, Department of Radiology, Mayo Clinic, 200 First St SW, Rochester, MN 55905, USA.
Email: Vemuri.Prashanthi@mayo.edu

Abstract

INTRODUCTION: Age-related and Alzheimer's disease (AD) dementia–related neurodegeneration impact brain health. While morphometric measures from T1-weighted scans are established biomarkers, they may be less sensitive to earlier changes. Neurite orientation dispersion and density imaging (NODDI), offering biologically meaningful interpretation of tissue microstructure, may be an advanced brain health biomarker.

METHODS: We contrasted regional gray matter NODDI and morphometric evaluations concerning their correlation with (1) age, (2) clinical diagnosis stage, and (3) tau pathology as assessed by AV1451 positron emission tomography.

RESULTS: Our study hypothesizes that NODDI measures are more sensitive to aging and early AD changes than morphometric measures. One NODDI output, free water fraction (FWF), showed higher sensitivity to age-related changes, generally better effect sizes in separating mild cognitively impaired from cognitively unimpaired participants, and stronger associations with regional tau deposition than morphometric measures.

DISCUSSION: These findings underscore NODDI's utility in capturing early neurodegenerative changes and enhancing our understanding of aging and AD.

KEYWORDS
brain aging, diffusion magnetic resonance imaging, early Alzheimer's disease dementia, neurite orientation dispersion and density imaging

Highlights

- Neurite orientation dispersion and density imaging can serve as an effective brain health biomarker for aging and early Alzheimer's disease (AD).
- Free water fraction has higher sensitivity to normal brain aging.
- Free water fraction has stronger associations with early AD and regional tau deposition.

1 | BACKGROUND

Brain health is influenced by multiple factors, such as genetics, sex, environment, lifestyle, and socioeconomic status. Worsening brain health is observed in the elderly due to both aging and pathology effects.[1] Recent evidence from imaging studies has shed light on brain changes observed due to brain aging and Alzheimer's disease (AD) suggesting that AD may have greater medial temporal involvement while aging changes are more widespread throughout the brain.[2–4] There is also increasing consensus that there are significant individual differences in brain changes.[5,6] Therefore, sensitive measurement of brain changes with aging and disease has important implications for understanding the mechanisms underlying these changes, early diagnosis, and intervention strategies.

While morphometry (from T1-weighted structural magnetic resonance imaging [MRI] scans) is widely accessible and commonly used for detecting neurodegeneration caused by aging and neurodegenerative pathologies, it may only inform about macroscopic structural changes and likely captures the later part of the disease process. While diffusion tensor imaging has been available for the measurement of microstructural integrity in aging[7,8] and AD dementia,[9] newer diffusion models such as neurite orientation dispersion and density imaging (NODDI) can provide a sensitive and more biologically specific interpretation of tissue microstructure.

NODDI relies on multishell diffusion MRI (dMRI) acquisition schemes and a biophysical model comprising intraneurite, extraneurite, and free water compartments.[10] "Neurites" correspond to axons and dendrites in brain tissue. NODDI provides unique information about neurite density, their angular dispersion, and the fraction of unrestricted ("free") water in voxels, represented as neurite density index (NDI), their orientation dispersion index (ODI), and isotropic water fraction or free water fraction (FWF). As a result, NODDI has the potential to capture subtle neurodegenerative changes caused by aging and pathology. Recent studies have shown that gray matter (GM) NODDI measures are exceptionally sensitive to aging throughout the brain,[11] and specifically show changes in early middle age in regions within and surrounding the hippocampus.[12,13] Additionally, NODDI measures are also associated with tau-related changes.[14]

In this article, we hypothesize that microstructural changes measured by NODDI, a biologically interpretable dMRI model, are more sensitive to neurodegeneration in aging and early-stage AD dementia compared to morphometric evaluations derived from T1 images. To test our hypothesis, we compared regional GM NODDI and morphometric measurements based on their association with (1) age, (2) clinical diagnosis stage (cognitively unimpaired [CU] participants vs. participants with mild cognitive impairment [MCI], CU vs. AD dementia), and (3) sensitivity to tau pathology measured using AV1451 positron emission tomography (PET). We investigated the usefulness of GM NODDI and morphometry in predicting in vivo measurements of mixed 3R/4R tau pathology in AD dementia in aim (3), as quantified using AV1451 PET, because tau pathology is proximal to clinical symptoms.[15]

RESEARCH IN CONTEXT

1. **Systematic Review**: We reviewed the literature using PubMed. Studies suggest advanced diffusion magnetic resonance imaging techniques, such as neurite orientation dispersion and density imaging (NODDI), offer additional microstructural insights beyond traditional morphometric measurements obtained from T1-weighted images. However, a comprehensive analysis on the effectiveness of gray matter NODDI in understanding aging and early Alzheimer's disease (AD) dementia compared to morphometric measures was lacking.
2. **Interpretation**: Our findings indicate that the free water fraction, a NODDI measurement (from multishell diffusion MRI), captures neurodegenerative changes associated with both aging and early-stage AD dementia.
3. **Future Directions**: The diagnostic potential of NODDI needs to be further explored using longitudinal studies, correlational analyses incorporating AD pathology and autopsy characterization, and through the development of comprehensive brain health markers that integrate various parameters into composite measures.

2 | METHODS

2.1 | Selection of participants and cohort description

We selected CU and MCI participants from a population-based cohort, the Mayo Clinic Study of Aging (MCSA). Additionally, we included patients clinically diagnosed with AD dementia (with age restriction of ≥ 65 years of age to limit to typical AD patients) from the Mayo Clinic Alzheimer's Disease Research Center (ADRC). The MCSA is a prospective epidemiology cohort aimed at investigating the prevalence, incidence, and risk factors for MCI and dementia.[16] MCSA participants were randomly selected and invited from Olmsted County in Minnesota. The population was enumerated using the Rochester Epidemiology Project medical records linkage system infrastructure.[17] participants underwent clinical diagnosis according to previously published criteria.[18]

The inclusion criteria were the availability of multishell dMRI (NODDI) measurements, morphometric measurements from T1-weighted scans, clinical diagnosis, and an accompanying AV1451 PET standardized uptake value ratio (SUVR) performed within 3 months of the MRI visit. Age was determined based on when the MRI scan occurred. Our final dataset consisted of 922 CU participants (564 of whom were amyloid and tau negative), 117 MCI participants, and 91 clinically diagnosed AD dementia patients (the AD dementia group comprised 4 individuals from MCSA and 87 from ADRC). The

TABLE 1 Participant characteristics including biographical data and imaging measurements.

Participant characteristics Mean (SD)	CU (n = 564) A–/T–	CU (n = 922)	MCI (n = 117)	AD dementia (n = 91)
Age, year	64.43 (12.79)	68.99 (12.82)	78.87 (9.79)	75.82 (6.53)
Males (%)	49.11%	50.54%	55.56%	51.65%
Education, year	15.49 (2.36)	15.44 (2.4)	13.69 (2.88)	15.91 (2.73)
MMSE	28.98 (1.02)	28.84 (1.09)	25.68 (2.08)	21.92 (4.60)
Imaging measures of AD				
PiB PET SUVR	1.36 (0.08)	1.54 (0.37)	1.85 (0.61)	2.44 (0.51)
AV1451 PET SUVR	1.15 (0.07)	1.20 (0.1)	1.28 (0.19)	1.77 (0.45)

Note: The percentages are reported for the categorical variables and the means (SDs) are reported for the continuous variables. Lowercase "n" denotes the number of participants. A–/T– indicates the amyloid-negative and tau-negative CU subgroup.

Abbreviations: AD, Alzheimer's disease; CU, cognitively unimpaired; MCI, mild cognitive impairment; MMSE, Mini-Mental State Examination; PET, positron emission tomography; PiB, Pittsburgh compound B; SD, standard deviation; SUVR, standardized uptake value ratio.

demographic and clinical characteristics of the study cohort are summarized in Table 1, with mean and standard deviation displayed for continuous variables and percentages for categorical variables.

2.2 | Standard protocol approvals, registrations, and patient consent

This study was approved by Mayo Clinic and Olmsted Medical Center institutional review boards. Written information was provided to all participants, and written consent was collected from all participants and qualified caregivers.

2.3 | Imaging methods

2.3.1 | MRI acquisition and processing

All MRIs were acquired on 3T Siemens Prisma scanners equipped with VE11 software and 64-channel receiver head coils. Structural scans were acquired with a magnetization-prepared rapid gradient echo (MPRAGE) sequence (repetition time [TR]/echo time [TE]/inversion time [TI] = 2300/3.14/945 ms, flip angle = 9°, isotropic resolution = 0.8 mm). Regional GM volumes and cortical thickness measurements were assessed using SPM12 segmentations from the TI-weighted MPRAGE images as described previously.[19] Regional GM volumes were normalized by total intracranial volume for each participant. Additionally, we calculated the mean values of thickness and volume of bilateral regions of interest (ROIs) in each brain region of the AAL122 GM atlas.

Diffusion scans were acquired with TR/TE = 3400/71 ms, field of view = 232 mm, voxel size = 2.0 mm isotropic, 81 axial slices, and consisted of 13 b = 0, 6 b = 500, 48 b = 1000, and 60 b = 2000 s/mm² volumes. Detailed acquisition protocols were published for MCSA previously.[20] dMRIs underwent denoising,[21] eddy current distortion and head motion correction,[22] Gibbs ringing correction,[23] and Rician debiasing.[24] The diffusion tensors were then fitted with a non-

linear least square fitting algorithm in dipy. NDI, ODI, and FWF maps were estimated by Accelerated Microstructure Imaging via Convex Optimization (AMICO). The diffusion images were transformed into native T1-w space using a warp calculated by Advanced Normalization Tools (ANTs) based on a quasi-T1-w image synthesized out of the diffusion data. Regional NODDI measures were obtained by warping the AAL122 GM atlas to participant native space using ANTs. We used a threshold of probability of GM > 0.5 (based on T1-based GM probability estimation) for diffusion measurements.

2.3.2 | Pittsburgh compound B PET and AV1451 PET imaging

Amyloid PET imaging was performed using Pittsburgh compound B (PiB) PET, and tau PET imaging was performed using AV1451 PET. Detailed acquisition, processing, and SUVR calculation procedures were previously described.[25] Global amyloid SUVR was computed by averaging the median uptake from prefrontal, orbitofrontal, parietal, temporal, anterior cingulate, and posterior cingulate/precuneus regions, then normalizing it by the median uptake in the cerebellar crus GM. We used a Centiloid value of 25 as the cutoff for brain amyloid positivity, which corresponds to PiB PET SUVR ≥ 1.52.[26]

From AV1451 PET scans, we computed median SUVRs of bilateral ROIs that mapped with the Braak staging scheme as described elsewhere.[27] In brief, the stages included the following regions: Braak I (transentorhinal cortex), Braak II (hippocampus), Braak III and IV (inferior and medial temporal cortex and posterior cingulum cortex), Braak V and VI (the isocortex of the frontal and parietal lobes). Notably, we excluded the Braak II region due to signal contamination from the choroid plexus.

Global tau SUVR was computed by averaging the median uptake from the amygdala, entorhinal cortex, fusiform gyrus, parahippocampal, inferior temporal, and middle temporal gyri regions, then normalized by the median uptake in the cerebellar crus GM. We used a previously determined cutoff of AV1451 PET SUVR ≥ 1.25 for tau positivity.[28]

2.3.3 | Cognitive performance

All MCSA and ADRC participants were administered the Short Test of Mental Status, the scores of which were transformed to Mini-Mental State Examination.[29]

2.4 | Statistical analyses

We conducted three experiments to illustrate the relative sensitivity of NODDI measures compared to morphometric measures in detecting neurodegeneration.

1. Correlation with age: We analyzed Spearman correlations, computed with the spearmanr function from scipy.stats package, between imaging measurements taken from the AAL122 atlas regions and chronological age in the amyloid-negative and tau-negative CU cohort. The confidence intervals (CIs) of Spearman correlations were derived by bootstrapping 564 amyloid-negative and tau-negative CU subgroups for 100 runs. This helped us pinpoint brain areas that are prone to changes associated with primarily age-related changes (independent of AD-related changes).

2. Effect sizes for clinical diagnostic groups: We compared regional imaging parameters between age-matched pairs of CU & MCI or CU & AD dementia participants. Age-matched pairs were created by pairing each participant with MCI or AD dementia with a CU participant whose age difference was within 1 year compared to the individual with MCI or AD dementia. The effect size of regional imaging parameters was evaluated with Cohen dz output by the ttest function in the researchpy package, with the assumption of matched samples and unequal variance. The MCI subgroup ($n = 117$) and AD subgroup ($n = 91$) were bootstrapped 100 times and paired with two age-matched CU cohorts ($n = 117$ and $n = 91$ for matching to MCI and AD groups, respectively) to minimize the influence of random sampling. Average values and CIs were reported for effect sizes. This comparison aimed to identify brain regions that display pathology-related neurodegeneration.

3. Prediction of regional AV1451 PET SUVR: we developed multivariable linear regression models to assess the predictive power of imaging metrics on AD pathology across brain regions. We segmented the brain into five ROIs according to Braak stages. For each Braak ROI, a multivariable linear regression model was fitted using the LinearRegression model from the sklearn package, with local AV1451 PET SUVR as the target variable and imaging parameters as predictors. Prior to model fitting, imaging measures, age, and AV1451 PET SUVR underwent preprocessing by Box–Cox and Z transformations.

2.5 | Regional importance illustrations

For ease of visualizing results, we generated brain maps with the AAL122 Atlas to demonstrate regional correlations with chronological age using MATLAB, vistasoft, mnl_ieegBasics, mnl_dmri_ieeg_tools, spm12, AFQ, and the ECoG electrode localization toolbox.

3 | RESULTS

3.1 | FWF and ODI have higher correlations with chronological age than morphometric measures

We investigated age-related changes in microstructural and morphometric measures using Spearman correlations within CU individuals. Our analysis, depicted in Figure 1, focused on identifying regional measurements that display strong associations with age, highlighting top-quartile Spearman correlations. For convenience, we will define the strength of Spearman correlation as follows: extremely weak (0.00–0.19), weak (0.20–0.39), moderate (0.40–0.59), strong (0.60–0.79), and very strong (0.80–1.00).

FWF exhibited widespread correlations with age. Strong Spearman correlations were observed in the temporal lobe, inferior occipital gyrus, parahippocampal region, and anterior cingulum. ODI showed moderate sensitivity in areas such as the frontal lobe, parietal lobe, central gray, sensorimotor cortex, and other scattered regions. In contrast, measures of cortical thickness and volume displayed only moderate correlations in Heschl gyrus and fusiform gyrus, respectively. NDI of the amygdala showed moderate correlations with age.

3.2 | FWF changes are more widespread in MCI and AD dementia

To assess the sensitivity of microstructural and morphometric measures in MCI and AD dementia, we compared effect sizes between age-matched CU and MCI participants (Figure 2, left), as well as between CU and AD dementia participants (Figure 2, right). To minimize the confounding influence of age, each MCI or AD dementia participant was paired with a CU participant within an age difference smaller than 1 year. To minimize the influence of random sampling, we repeated the computation 100 times and reported average effect sizes. Effect sizes were quantified using Cohen dz, enabling a direct comparison of changes across different imaging measures. We will define the strength of Cohen dz as follows: low (0.2), moderate (0.5), high (0.8).

In the comparison between CU and MCI participants, FWF exhibited slightly larger effect sizes in many more regions compared to other measures, with the most notable effects seen in the frontal lobe, temporal lobe, medial temporal lobe (MTL), and anterior cingulum. Conversely, volumetric measures displayed moderate to low effect sizes in the temporal lobe, MTL, and various isolated regions. ODI showed changes across dispersed regions, while NDI demonstrated the most substantial change in the MTL. The most pronounced change in cortical thickness was observed in the insula.

Due to the greater separation of disease stage between CU and AD dementia participants, there were more significant differences in most of the tested brain measures. FWF displayed a larger overall effect size
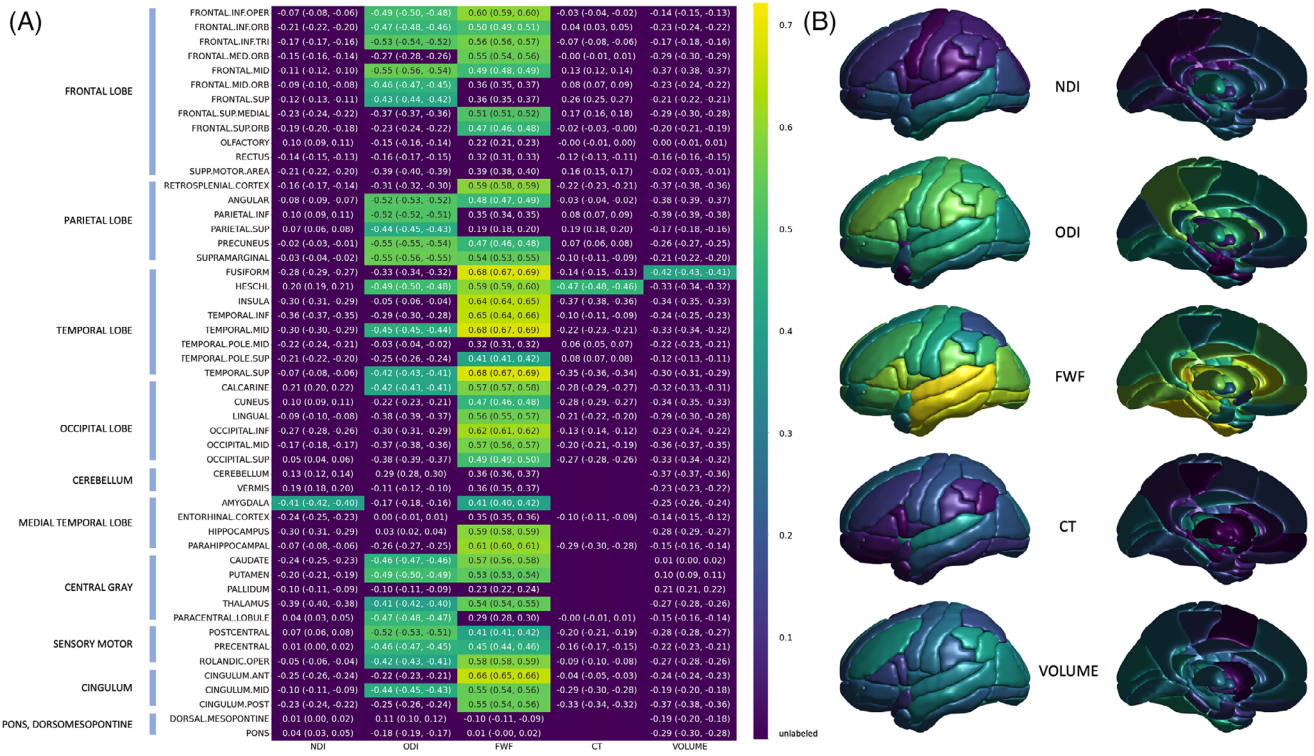
(A)

Lobe	Region	NDI	ODI	FWF	CT	VOLUME
FRONTAL LOBE	FRONTAL.INF.OPER	-0.07 (-0.08, -0.06)	-0.49 (-0.50, -0.48)	0.60 (0.59, 0.60)	-0.03 (-0.04, -0.02)	-0.14 (-0.15, -0.13)
	FRONTAL.INF.ORB	-0.21 (-0.22, -0.20)	-0.47 (-0.48, -0.46)	0.50 (0.49, 0.51)	0.04 (0.03, 0.05)	-0.23 (-0.24, -0.22)
	FRONTAL.INF.TRI	-0.17 (-0.17, -0.16)	-0.53 (-0.54, -0.52)	0.56 (0.56, 0.57)	-0.07 (-0.08, -0.06)	-0.17 (-0.18, -0.16)
	FRONTAL.MED.ORB	-0.15 (-0.16, -0.14)	-0.27 (-0.28, -0.26)	0.55 (0.54, 0.56)	-0.00 (-0.01, 0.01)	-0.29 (-0.30, -0.29)
	FRONTAL.MID	0.11 (0.12, 0.10)	0.55 (0.56, 0.54)	0.49 (0.48, 0.49)	0.13 (0.12, 0.14)	0.37 (0.38, 0.37)
	FRONTAL.MID.ORB	-0.09 (-0.10, -0.08)	-0.46 (-0.47, -0.45)	0.36 (0.35, 0.37)	0.08 (0.07, 0.09)	-0.23 (-0.24, -0.22)
	FRONTAL.SUP	0.12 (0.13, 0.11)	0.43 (0.44, 0.42)	0.36 (0.35, 0.37)	0.26 (0.25, 0.27)	0.21 (0.22, 0.20)
	FRONTAL.SUP.MEDIAL	-0.23 (-0.24, -0.22)	-0.37 (-0.37, -0.36)	0.51 (0.51, 0.52)	0.17 (0.16, 0.18)	-0.29 (-0.30, -0.28)
	FRONTAL.SUP.ORB	-0.19 (-0.20, -0.18)	-0.23 (-0.24, -0.22)	0.47 (0.46, 0.48)	-0.02 (-0.03, -0.00)	-0.20 (-0.21, -0.19)
	OLFACTORY	0.10 (0.09, 0.11)	-0.15 (-0.16, -0.14)	0.22 (0.21, 0.23)	-0.00 (-0.01, 0.00)	0.00 (-0.01, 0.01)
	RECTUS	-0.14 (-0.15, -0.13)	-0.16 (-0.17, -0.15)	0.32 (0.31, 0.33)	-0.12 (-0.13, -0.11)	-0.16 (-0.16, -0.15)
	SUPP.MOTOR.AREA	-0.21 (-0.22, -0.20)	-0.39 (-0.40, -0.39)	0.39 (0.38, 0.40)	0.16 (0.15, 0.17)	-0.02 (-0.03, -0.01)
PARIETAL LOBE	RETROSPLENIAL.CORTEX	-0.16 (-0.17, -0.14)	-0.31 (-0.32, -0.30)	0.59 (0.58, 0.59)	-0.22 (-0.23, -0.21)	-0.37 (-0.38, -0.36)
	ANGULAR	0.08 (0.09, 0.07)	0.52 (0.53, 0.52)	0.48 (0.47, 0.49)	0.03 (0.04, 0.02)	0.38 (0.39, 0.37)
	PARIETAL.INF	0.10 (0.09, 0.11)	-0.52 (-0.52, -0.51)	0.35 (0.34, 0.35)	0.08 (0.07, 0.09)	-0.39 (-0.39, -0.38)
	PARIETAL.SUP	0.07 (0.06, 0.08)	-0.44 (-0.45, -0.43)	0.19 (0.18, 0.20)	0.19 (0.18, 0.20)	-0.17 (-0.18, -0.16)
	PRECUNEUS	-0.02 (-0.03, -0.01)	-0.55 (-0.55, -0.54)	0.47 (0.46, 0.48)	0.07 (0.06, 0.08)	-0.26 (-0.27, -0.25)
	SUPRAMARGINAL	-0.03 (-0.04, -0.02)	-0.55 (-0.56, -0.55)	0.54 (0.53, 0.55)	-0.10 (-0.11, -0.09)	-0.21 (-0.22, -0.20)
TEMPORAL LOBE	FUSIFORM	-0.28 (-0.29, -0.27)	-0.33 (-0.34, -0.32)	0.68 (0.67, 0.69)	-0.14 (-0.15, -0.13)	-0.42 (-0.43, -0.41)
	HESCHL	0.20 (0.19, 0.21)	-0.49 (-0.50, -0.48)	0.59 (0.59, 0.60)	-0.47 (-0.48, -0.46)	-0.33 (-0.34, -0.32)
	INSULA	0.30 (0.31, 0.29)	0.05 (0.06, 0.04)	0.64 (0.64, 0.65)	-0.37 (-0.38, -0.36)	0.34 (0.35, 0.33)
	TEMPORAL.INF	-0.36 (-0.37, -0.35)	-0.29 (-0.30, -0.28)	0.65 (0.64, 0.66)	-0.10 (-0.11, -0.09)	-0.24 (-0.25, -0.23)
	TEMPORAL.MID	-0.30 (-0.30, -0.29)	-0.45 (-0.45, -0.44)	0.68 (0.67, 0.69)	-0.22 (-0.23, -0.21)	-0.33 (-0.34, -0.32)
	TEMPORAL.POLE.MID	-0.22 (-0.24, -0.21)	-0.03 (-0.04, -0.02)	0.32 (0.31, 0.32)	0.06 (0.05, 0.07)	-0.22 (-0.23, -0.21)
	TEMPORAL.POLE.SUP	-0.21 (-0.22, -0.20)	-0.25 (-0.26, -0.24)	0.41 (0.41, 0.42)	0.08 (0.07, 0.08)	-0.12 (-0.13, -0.11)
	TEMPORAL.SUP	-0.07 (-0.08, -0.06)	-0.42 (-0.43, -0.41)	0.68 (0.67, 0.69)	-0.35 (-0.36, -0.34)	-0.30 (-0.31, -0.29)
OCCIPITAL LOBE	CALCARINE	0.21 (0.20, 0.22)	-0.42 (-0.43, -0.41)	0.57 (0.57, 0.58)	-0.28 (-0.29, -0.27)	-0.32 (-0.33, -0.31)
	CUNEUS	0.10 (0.09, 0.11)	-0.22 (-0.23, -0.21)	0.47 (0.46, 0.48)	0.28 (0.29, 0.27)	0.34 (0.35, 0.33)
	LINGUAL	-0.09 (-0.10, -0.08)	-0.38 (-0.39, -0.37)	0.56 (0.55, 0.57)	-0.21 (-0.22, -0.20)	-0.29 (-0.30, -0.28)
	OCCIPITAL.INF	0.27 (0.28, 0.26)	0.30 (0.31, 0.29)	0.62 (0.61, 0.62)	0.13 (0.14, 0.12)	0.23 (0.24, 0.22)
	OCCIPITAL.MID	-0.17 (-0.18, -0.17)	-0.37 (-0.38, -0.36)	0.57 (0.56, 0.57)	-0.20 (-0.21, -0.19)	-0.36 (-0.37, -0.35)
	OCCIPITAL.SUP	0.05 (0.04, 0.06)	-0.38 (-0.39, -0.37)	0.49 (0.49, 0.50)	-0.27 (-0.28, -0.26)	-0.33 (-0.34, -0.32)
CEREBELLUM	CEREBELLUM	0.13 (0.12, 0.14)	0.29 (0.28, 0.30)	0.36 (0.36, 0.37)		-0.37 (-0.37, -0.36)
	VERMIS	0.19 (0.18, 0.20)	-0.11 (-0.12, -0.10)	0.36 (0.35, 0.37)		-0.23 (-0.23, -0.22)
MEDIAL TEMPORAL LOBE	AMYGDALA	-0.41 (-0.42, -0.40)	-0.17 (-0.18, -0.16)	0.41 (0.40, 0.42)		-0.25 (-0.26, -0.24)
	ENTORHINAL.CORTEX	-0.24 (-0.25, -0.23)	0.00 (-0.01, 0.01)	0.35 (0.35, 0.36)	-0.10 (-0.11, -0.12)	-0.14 (-0.15, -0.12)
	HIPPOCAMPUS	0.30 (0.31, 0.29)	0.03 (0.02, 0.04)	0.59 (0.58, 0.59)		-0.28 (-0.29, -0.27)
	PARAHIPPOCAMPAL	-0.07 (-0.08, -0.06)	-0.26 (-0.27, -0.24)	0.61 (0.60, 0.61)	-0.29 (-0.30, -0.28)	-0.15 (-0.16, -0.14)
CENTRAL GRAY	CAUDATE	-0.24 (-0.25, -0.23)	-0.46 (-0.47, -0.46)	0.57 (0.56, 0.58)		0.01 (0.00, 0.02)
	PUTAMEN	-0.20 (-0.21, -0.19)	-0.49 (-0.50, -0.49)	0.53 (0.53, 0.54)		0.10 (0.09, 0.11)
	PALLIDUM	-0.10 (-0.11, -0.09)	-0.10 (-0.11, -0.09)	0.23 (0.22, 0.24)		0.21 (0.21, 0.22)
	THALAMUS	-0.39 (-0.40, -0.38)	0.41 (0.42, 0.40)	0.54 (0.54, 0.55)		-0.27 (-0.28, -0.26)
SENSORY MOTOR	PARACENTRAL.LOBULE	0.04 (0.03, 0.05)	-0.47 (-0.48, -0.47)	0.29 (0.28, 0.30)	-0.00 (-0.01, 0.01)	-0.15 (-0.16, -0.14)
	POSTCENTRAL	0.07 (0.06, 0.08)	0.52 (0.53, 0.51)	0.41 (0.41, 0.42)	-0.20 (-0.21, -0.19)	-0.28 (-0.28, -0.27)
	PRECENTRAL	0.01 (0.00, 0.02)	-0.46 (-0.47, -0.45)	0.45 (0.44, 0.46)	-0.16 (-0.17, -0.15)	-0.22 (-0.23, -0.21)
	ROLANDIC.OPER	0.05 (0.06, -0.04)	-0.42 (-0.43, -0.41)	0.58 (0.58, 0.59)	-0.09 (-0.10, -0.08)	-0.22 (-0.23, -0.21)
CINGULUM	CINGULUM.ANT	-0.25 (-0.26, -0.24)	-0.22 (-0.23, -0.21)	0.66 (0.65, 0.66)	-0.04 (-0.05, -0.03)	-0.24 (-0.24, -0.23)
	CINGULUM.MID	-0.10 (-0.11, -0.09)	-0.44 (-0.45, -0.43)	0.55 (0.54, 0.56)	-0.29 (-0.30, -0.28)	-0.37 (-0.38, -0.36)
	CINGULUM.POST	-0.23 (-0.24, -0.22)	-0.25 (-0.26, -0.24)	0.55 (0.54, 0.56)	-0.33 (-0.34, -0.32)	-0.37 (-0.38, -0.36)
PONS, DORSOMESOPONTINE	DORSAL.MESOPONTINE	0.01 (0.00, 0.02)	0.11 (0.10, 0.12)	-0.10 (-0.11, -0.09)		-0.19 (-0.20, -0.18)
	PONS	0.04 (0.03, 0.05)	-0.18 (-0.19, -0.17)	0.01 (-0.00, 0.02)		-0.29 (-0.30, -0.28)

(B)

NDI

ODI

FWF

CT

VOLUME

FIGURE 1 A, Heatmap of Spearman correlations between regional imaging measurements and chronological age within CU participants. Spearman correlations were reported as mean (lower bound of 95% CI, upper bound of 95% CI) from 100 bootstrapping runs. Heatmap colors were coded based on the absolute value of the mean correlation coefficients. Only regions with Spearman correlations in the top quartile are colored for clarity. Yellow color indicates correlations with high magnitude. B, Visual representation of regional Spearman correlations as illustrated in (A). CI, confidence interval; CT, cortical thickness and gray matter volume; CU, cognitively unimpaired; FWF, free water fraction; NDI, neurite density index; ODI, orientation dispersion index.

across most GM regions, particularly in the temporal lobe and MTL. Volumes of MTL and temporal lobe exhibited comparable effect sizes to FWF of these areas. ODI changes were moderate–high across dispersed regions such as the parahippocampal cortex, fusiform gyrus, and middle cingulum. NDI changes were most prominent in the inferior temporal gyrus and MTL. Cortical thickness changes were evident in the temporal lobe, MTL, posterior cingulum, and retrosplenial cortex.

These findings suggest that microstructural measurements provided by NODDI, particularly FWF, may serve as promising biomarkers for pathological neurodegeneration.

3.3 | Free water measurements outperform other measures in prediction models of tau pathology in Braak ROIs I, III–V

Multivariable linear regression models were fitted for each Braak ROI, incorporating microstructural measures, morphometric measures, age, and sex as regressors. Figure 3 illustrates the β coefficients and their corresponding CIs.

FWF exhibited the overall highest magnitude of β coefficients among the imaging measures, followed by ODI. Volumes, cortical thickness, and NDI showed smaller β coefficients across the ROIs. Model R^2 values indicated better fits for Braak ROI I, III, IV, suggesting a stronger

association between tau deposition and the included imaging measures in these regions.

4 | DISCUSSION

Neurodegeneration biomarkers, particularly MRI-based morphometric measurements, are widely used to quantify brain health and assist in the diagnosis of AD. In this study, we assessed the sensitivity of microstructural and morphometric measures within GM to capture neurodegenerative changes associated with aging and AD dementia. Our findings highlighted the potential of FWF (cortical tissue free water content) as a promising biomarker for GM health. Specifically, we found that (1) FWF exhibited the highest correlations with chronological age across the amyloid-negative and tau-negative CU cohort, (2) FWF provided better overall effect sizes in identifying MCI participants, and (3) FWF demonstrated stronger associations than other tested measures with tau deposition in multiple brain regions.

4.1 | GM microstructural changes and their relevance to age-related neurodegeneration

NODDI provides precise measurements of brain tissue microstructure by modeling three compartments within each voxel: intracellular,
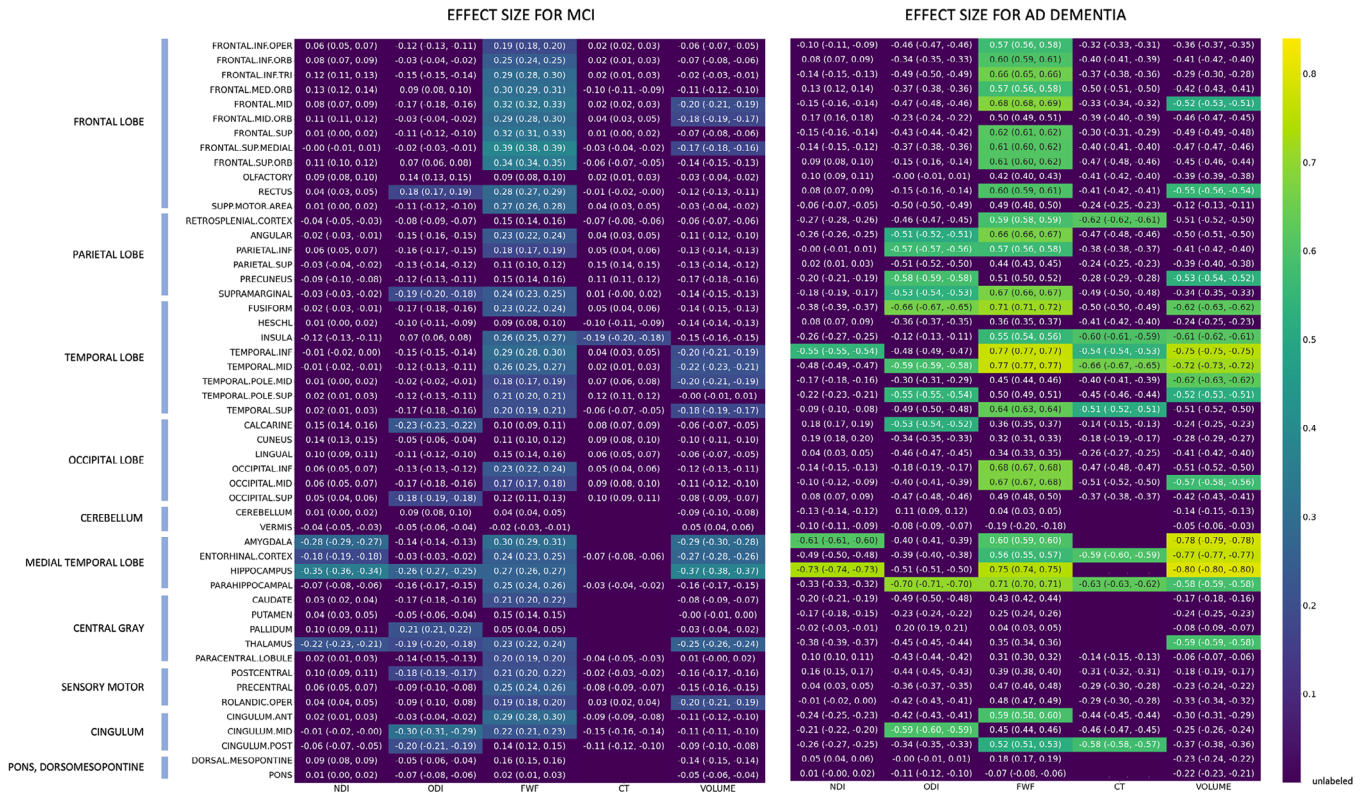
FIGURE 2 Heatmap displaying average effect sizes (Cohen dz) indicating the disparity in microstructural and morphometric measures between age-matched CU and participants with MCI (left), as well as between CU and AD dementia participants (right). Effect sizes were reported as mean (lower bound of 95% CI, upper bound of 95% CI) from 100 bootstrapping runs. Heatmap colors were assigned based on the absolute value of effect sizes. Only regions with absolute Cohen dz values in the top quartile are color-coded for clarity. Yellow color indicates larger effect size, thus more significant change between the CU group and the compared group. AD, Alzheimer's disease; CI, confidence interval; CT, cortical thickness and gray matter volume; CU, cognitively unimpaired; FWF, free water fraction; MCI, mild cognitive impairment; NDI, neurite density index; ODI, orientation dispersion index.
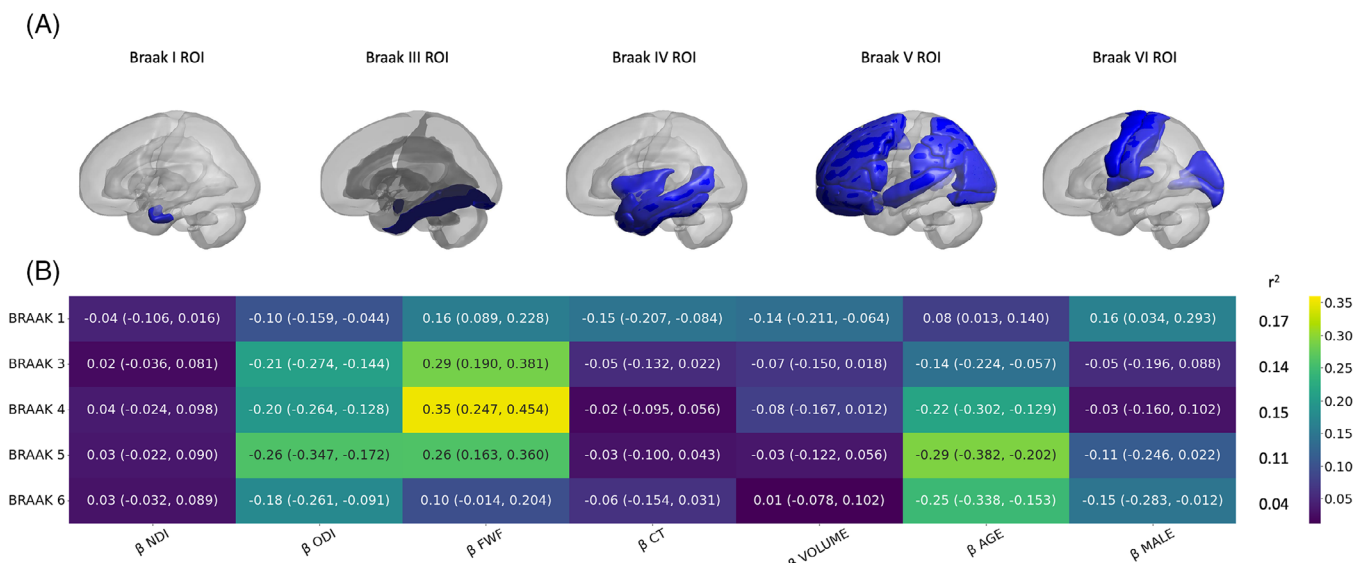
FIGURE 3 A, Illustrations of Braak ROIs I, III–VI. B, Multivariable linear regression models are fit to each Braak stage ROI. For each ROI, imaging parameters serve as regressors and tau deposition as the target. Colors are assigned based on the absolute value of linear coefficients. CT, cortical thickness and gray matter volume; FWF, free water fraction; NDI, neurite density index; ODI, orientation dispersion index; ROI, region of interest.

extracellular, and free water. These compartments represent different microstructural spaces: the intracellular compartment includes water restricted to one-dimensional diffusion (e.g., water confined within neurites); the extracellular compartment encompasses spaces between neurites or within spherical cell bodies, where diffusion is hindered by extracellular structures; and the free water compartment consists of water that did not encounter barriers during diffusion, such as cerebrospinal fluid or any water farther than ≈ 10 μm from a membrane.[10] Hence, by quantifying neurite morphology, NODDI can reveal the structural basis of brain function. For example, through FWF, it separates complete tissue loss (atrophy) from within-tissue microstructural changes (NDI and ODI). In cortical areas affected by aging and neurodegenerative disorders, NODDI demonstrates its capability to detect features of brain tissue deterioration, including neuronal loss,[30–32] neurite degeneration,[32,33] and demyelination,[34,35] all of which have been previously examined using histology, along with the subsequent increase in FWF.[36–40] Based on this literature, microstructural changes reported by NODDI have the potential to become additional GM health biomarkers. Figure 1 showed an increase in FWF across most GM regions with aging, as suggested by Merluzzi et al.[11] Additionally, our analysis provides a region-corresponding comparison of age correlations between NODDI-derived and T1-derived metrics, supporting the argument that FWF exhibits the greatest sensitivity to age among these metrics. Therefore, microstructural measures may be more sensitive to age-related neurodegeneration, and they outperform morphometric measures in this aspect. Our study also showed a smaller, but widespread negative association of ODI with age in the parietal lobe, frontal lobe, central gray, sensorimotor cortex, cingulum, and scattered locations in the temporal lobe, which corresponds to the fronto-parietal decreasing ODI pattern observed with aging previously.[41] Among T1-weighted metrics, the volume of fusiform gyrus and cortical thickness of the Heschl gyrus showed the strongest negative correlations with age. Other regional T1 metrics with comparatively more prominent age correlations are scattered throughout the brain. Our observations partially deviate from the frontal–temporal pattern described in other studies,[3] likely because we excluded amyloid- or tau-positive participants from our analysis cohort to control for the effect of AD pathology, despite them being CU. The correlation coefficients for T1-derived metrics generally decreased after removing pathology-positive CU participants from analysis cohort (data not shown).

4.2 | Earlier change in GM microstructural free water and its relevance in MCI/AD dementia

While it is recognized that there is considerable variability of atrophy seen in AD, hippocampal atrophy is observed in a majority of typical late-onset AD patients.[42] Our findings in the right panel of Figure 2 corroborate previous observations, showing significant differences in hippocampal volumes between age-matched CU and AD dementia

participants, with an effect size of −0.8. Hippocampal FWF demonstrated comparable efficacy to volume measurement, with an effect size of 0.75. Both volume and FWF of the medial and inferior temporal lobe show high effect sizes of similar magnitude. Although FWF and volume show similar effect sizes, FWF displays more significant correlations across more GM regions. However, it is important to point out that hippocampal atrophy is non-specific to AD. Different pathologies have been shown to affect hippocampal atrophy.[43] It has been shown that anterior MTL regions are strongly associated with TAR DNA-binding protein 43, whereas the posterior hippocampus is associated with tau.[44] Therefore, our measured changes may be broader than AD alone.

FWF may be a promising biomarker in the earlier stages of cognitive impairment. Previous dMRI studies have shown that microstructural alterations precede macroscopic changes, correlating with regional dysfunction and having the potential to predict future progression into AD dementia.[45–47] Our findings, as depicted in the left panel of Figure 2, indicate a greater number of regions with changes in FWF compared to morphometric measures. Moreover, the magnitudes of FWF changes tended to be slightly higher. For instance, the effect size of FWF from the frontal, parietal, and temporal lobes surpassed those of corresponding volumes. However, FWF measurements in the MTL are comparable to MTL volumes. These results suggest that cortical microstructural changes reflected by FWF may precede macrostructural changes in more brain regions, highlighting its potential as a sensitive assessment tool for the neurodegenerative process, especially when using holistic methods (e.g., brain age models) that consider all brain regions at once. Nevertheless, further studies are needed to determine the specificity of FWF to AD pathology and its correlation with autopsy characterization, for example, Braak staging.

Overall, in CU/AD comparison, FWF shows relatively high positive changes across regions, with the strongest effect size seen in temporal lobes and MTL. In comparison, NDI had smaller effect sizes in most GM areas except for the MTL. Vogt et al. focused on NDI and ODI and found changes throughout temporal and parietal cortical regions in MCI and AD.[48] While their ODI findings are similar to those of our study, the differences in NDI may be likely due to participant and cohort characteristics. The MCI and AD participants included in our study have older ages because of the sampling from the population and focus on only late-onset AD.

4.3 | GM FWF association with tau pathology

The relationship between GM microstructural measures and tau deposition in AD dementia is less studied compared to white matter microstructural or morphometric measures. Previous studies either focused on specific areas, such as MTL,[49] or used less biologically interpretable dMRI methods.[50] Our findings in Figure 3 suggest that FWF may provide the most predictive power for tau deposition in our multivariable linear regression models across multiple brain regions among all microstructural and morphometric measures.

4.4 | Usefulness of NODDI in aging and dementia studies

Our findings support the use of non-invasive, accessible biophysical diffusion models to indicate GM deterioration from aging and AD dementia. With multiband acceleration becoming more widespread, these models can illuminate cognitive decline causes, aiding early disease detection and monitoring. Future studies will refine NODDI's application in distinguishing diagnoses and tracking GM damage over time as diseases evolve.

4.5 | Strengths and limitations

This study's strengths include integrating NODDI, T1-weighted MRI, and tau neuroimaging measures, providing biologically interpretable insights into neurodegenerative changes. Comparing microstructural and morphometric measures within the same brain regions allowed us to assess the sensitivity of each imaging measure and relevant brain subregions in a comprehensive fashion. While we suggest that microstructural changes detected by NODDI may precede morphometric changes, longitudinal studies will be needed in validating this finding and exploring these measures as biomarkers. The comparison of NODDI and other diffusion modalities is also a valuable direction for future exploration.

CONFLICT OF INTEREST STATEMENT

The authors declare no conflicts of interest. Author disclosures are available in the supporting information.

CONSENT STATEMENT

Written information was provided to all participants, and written consent was collected from all participants and qualified caregivers.

ORCID

Xi Yu https://orcid.org/0000-0002-1024-4653

REFERENCES

1. Bethlehem RAI, Seidlitz J, White SR, et al. Brain charts for the human lifespan. *Nature*. 2022;604(7906):525-533.
2. Bakkour A, Morris JC, Wolk DA, Dickerson BC. The effects of aging and Alzheimer's disease on cerebral cortical anatomy: specificity and differential relationships with cognition. *Neuroimage*. 2013;76: 332-344.
3. Fjell AM, McEvoy L, Holland D, Dale AM, Walhovd KB. Alzheimer's Disease Neuroimaging I. What is normal in normal aging? Effects of aging, amyloid and Alzheimer's disease on the cerebral cortex and the hippocampus. *Prog Neurobiol*. 2014;117:20-40.
4. Hwang G, Abdulkadir A, Erus G, et al. Disentangling Alzheimer's disease neurodegeneration from typical brain ageing using machine learning. *Brain Commun*. 2022;4(3):fcac117.
5. Neth BJ, Graff-Radford J, Mielke MM, et al. Relationship between risk factors and brain reserve in late middle age: implications for cognitive aging. *Front Aging Neurosci*. 2019;11:355.
6. Walhovd KB, Lovden M, Fjell AM. Timing of lifespan influences on brain and cognition. *Trends Cogn Sci*. 2023;27(10):901-915.
7. Sullivan EV, Pfefferbaum A. Diffusion tensor imaging and aging. *Neurosci Biobehav Rev*. 2006;30(6):749-761.
8. Salminen LE, Conturo TE, Laidlaw DH, et al. Regional age differences in gray matter diffusivity among healthy older adults. *Brain Imaging Behav*. 2016;10(1):203-211.
9. Oishi K, Mielke MM, Albert M, Lyketsos CG, Mori S. DTI analyses and clinical applications in Alzheimer's disease. *J Alzheimers Dis*. 2011;26 Suppl 3(3):287-296. Suppl.
10. Zhang H, Schneider T, Wheeler-Kingshott CA, Alexander DC. NODDI: practical in vivo neurite orientation dispersion and density imaging of the human brain. *Neuroimage*. 2012;61(4):1000-1016.
11. Merluzzi AP, Dean DC 3rd, Adluru N, et al. Age-dependent differences in brain tissue microstructure assessed with neurite orientation dispersion and density imaging. *Neurobiol Aging*. 2016;43: 79-88.
12. Venkatesh A, Stark SM, Stark CEL, Bennett IJ. Age- and memory-related differences in hippocampal gray matter integrity are better captured by NODDI compared to single-tensor diffusion imaging. *Neurobiol Aging*. 2020;96:12-21.
13. Radhakrishnan H, Stark SM, Stark CEL. Microstructural alterations in hippocampal subfields mediate age-related memory decline in humans. *Front Aging Neurosci*. 2020;12:94.
14. Colgan N, Siow B, O'Callaghan JM, et al. Application of neurite orientation dispersion and density imaging (NODDI) to a tau pathology model of Alzheimer's disease. *Neuroimage*. 2016;125:739-744.
15. Samudra N, Lane-Donovan C, VandeVrede L, Boxer AL. Tau pathology in neurodegenerative disease: disease mechanisms and therapeutic avenues. *J Clin Invest*. 2023;133(12):e168553.
16. Roberts RO, Geda YE, Knopman DS, et al. The Mayo Clinic Study of Aging: design and sampling, participation, baseline measures and sample characteristics. *Neuroepidemiology*. 2008;30(1):58-69.
17. St Sauver JL, Grossardt BR, Yawn BP, et al. Data resource profile: the Rochester Epidemiology Project (REP) medical records-linkage system. *Int J Epidemiol*. 2012;41(6):1614-1624.
18. Petersen RC, Roberts RO, Knopman DS, et al. Prevalence of mild cognitive impairment is higher in men. The Mayo Clinic Study of Aging. *Neurology*. 2010;75(10):889-897.
19. Schwarz CG, Gunter JL, Wiste HJ, et al. A large-scale comparison of cortical thickness and volume methods for measuring Alzheimer's disease severity. *Neuroimage Clin*. 2016;11:802-812.
20. Raghavan S, Reid RI, Przybelski SA, et al. Diffusion models reveal white matter microstructural changes with ageing, pathology and cognition. *Brain Commun*. 2021;3(2):fcab106.
21. Veraart J, Novikov DS, Christiaens D, Ades-Aron B, Sijbers J, Fieremans E. Denoising of diffusion MRI using random matrix theory. *Neuroimage*. 2016;142:394-406.
22. Andersson JLR, Sotiropoulos SN. An integrated approach to correction for off-resonance effects and subject movement in diffusion MR imaging. *Neuroimage*. 2016;125:1063-1078.

23. Kellner E, Dhital B, Kiselev VG, Reisert M. Gibbs-ringing artifact removal based on local subvoxel-shifts. *Magn Reson Med.* 2016;76(5):1574-1581.

24. Koay CG, Ozarslan E, Basser PJ. A signal transformational framework for breaking the noise floor and its applications in MRI. *J Magn Reson.* 2009;197(2):108-119.

25. Jack CR Jr, Wiste HJ, Weigand SD, et al. Defining imaging biomarker cut points for brain aging and Alzheimer's disease. *Alzheimers Dement.* 2017;13(3):205-216.

26. Hu Y, Kirmess KM, Meyer MR, et al. Assessment of a plasma amyloid probability score to estimate amyloid positron emission tomography findings among adults with cognitive impairment. *JAMA Netw Open.* 2022;5(4):e228392.

27. Tian J, Raghavan S, Reid RI, et al. White matter degeneration pathways associated with tau deposition in Alzheimer disease. *Neurology.* 2023;100(22):e2269-e2278.

28. Jack CR Jr, Wiste HJ, Therneau TM, et al. Associations of amyloid, tau, and neurodegeneration biomarker profiles with rates of memory decline among individuals without dementia. *JAMA.* 2019;321(23):2316-2325.

29. Folstein MF, Folstein SE, McHugh PR. "Mini-mental state". A practical method for grading the cognitive state of patients for the clinician. *J Psychiatr Res.* 1975;12(3):189-198.

30. Pannese E. Morphological changes in nerve cells during normal aging. *Brain Struct Funct.* 2011;216(2):85-89.

31. Goel P, Chakrabarti S, Goel K, Bhutani K, Chopra T, Bali S. Neuronal cell death mechanisms in Alzheimer's disease: an insight. *Front Mol Neurosci.* 2022;15:937133.

32. Castelli V, Benedetti E, Antonosante A, et al. Neuronal cells rearrangement during aging and neurodegenerative disease: metabolism, oxidative stress and organelles dynamic. *Front Mol Neurosci.* 2019;12:132.

33. Dorostkar MM, Zou C, Blazquez-Llorca L, Herms J. Analyzing dendritic spine pathology in Alzheimer's disease: problems and opportunities. *Acta Neuropathol.* 2015;130(1):1-19.

34. Flynn SW, Lang DJ, Mackay AL, et al. Abnormalities of myelination in schizophrenia detected in vivo with MRI, and post-mortem with analysis of oligodendrocyte proteins. *Mol Psychiatry.* 2003;8(9):811-820.

35. Kolasinski J, Stagg CJ, Chance SA, et al. A combined post-mortem magnetic resonance imaging and quantitative histological study of multiple sclerosis pathology. *Brain.* 2012;135(10):2938-2951. Pt.

36. Cao M, Luo Y, Wu Z, Wu K, Li X. Abnormal neurite density and orientation dispersion in frontal lobe link to elevated hyperactive/impulsive behaviours in young adults with traumatic brain injury. *Brain Commun.* 2022;4(1):fcac011.

37. Parker TD, Slattery CF, Zhang J, et al. Cortical microstructure in young onset Alzheimer's disease using neurite orientation dispersion and density imaging. *Hum Brain Mapp.* 2018;39(7):3005-3017.

38. Fu X, Shrestha S, Sun M, et al. Microstructural white matter alterations in mild cognitive impairment and Alzheimer's disease : study based on neurite orientation dispersion and density imaging (NODDI). *Clin Neuroradiol.* 2020;30(3):569-579.

39. Gozdas E, Fingerhut H, Dacorro L, Bruno JL, Hosseini SMH. Neurite imaging reveals widespread alterations in gray and white matter neurite morphology in healthy aging and amnestic mild cognitive impairment. *Cereb Cortex.* 2021;31(12):5570-5578.

40. Andica C, Kamagata K, Kirino E, et al. Neurite orientation dispersion and density imaging reveals white matter microstructural alterations in adults with autism. *Mol Autism.* 2021;12(1):48.

41. Nazeri A, Chakravarty MM, Rotenberg DJ, et al. Functional consequences of neurite orientation dispersion and density in humans across the adult lifespan. *J Neurosci.* 2015;35(4):1753-1762.

42. Ferreira D, Nordberg A, Westman E. Biological subtypes of Alzheimer disease: a systematic review and meta-analysis. *Neurology.* 2020;94(10):436-448.

43. Yu L, Boyle PA, Dawe RJ, Bennett DA, Arfanakis K, Schneider JA. Contribution of TDP and hippocampal sclerosis to hippocampal volume loss in older-old persons. *Neurology.* 2020;94(2):e142-e152.

44. de Flores R, Wisse LEM, Das SR, et al. Contribution of mixed pathology to medial temporal lobe atrophy in Alzheimer's disease. *Alzheimers Dement.* 2020;16(6):843-852.

45. Ringman JM, O'Neill J, Geschwind D, et al. Diffusion tensor imaging in preclinical and presymptomatic carriers of familial Alzheimer's disease mutations. *Brain.* 2007;130:1767-1776.

46. Kantarci K, Petersen RC, Boeve BF, et al. DWI predicts future progression to Alzheimer disease in amnestic mild cognitive impairment. *Neurology.* 2005;64(5):902-904.

47. Muller MJ, Greverus D, Dellani PR, et al. Functional implications of hippocampal volume and diffusivity in mild cognitive impairment. *Neuroimage.* 2005;28(4):1033-1042.

48. Vogt NM, Hunt JF, Adluru N, et al. Cortical microstructural alterations in mild cognitive impairment and Alzheimer's disease dementia. *Cereb Cortex.* 2020;30(5):2948-2960.

49. Weston PSJ, Coath W, Harris MJ, et al. Cortical tau is associated with microstructural imaging biomarkers of neurite density and dendritic complexity in Alzheimer's disease. *Alzheimers Dement.* 2023;19(6):2750-2754.

50. Lee P, Kim HR, Jeong Y. Alzheimer's Disease Neuroimaging I. Detection of gray matter microstructural changes in Alzheimer's disease continuum using fiber orientation. *BMC Neurol.* 2020;20(1):362.

SUPPORTING INFORMATION

Additional supporting information can be found online in the Supporting Information section at the end of this article.